Geochemical Perspectives Letters

A partial melting control on the Zn isotope composition of basalts

J.M.D. Day[1,2*], F. Moynier[2], O. Ishizuka[3]

OPEN ACCESS

https://doi.org/10.7185/geochemlet.2230

Abstract

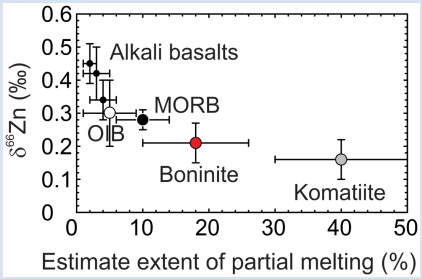

Basaltic partial melts are produced in a range of tectonic settings, including fluid-assisted melting above subduction zones, decompression melting at ridges and thermally driven melting above mantle plumes. To examine the role of partial melting on Zn, isotope and abundance data are reported for modern large-degree partial melts of the mantle represented by 22 mid-ocean ridge basalts (MORB) from three ocean basins and the first data for boninites. Boninites have some of the lowest Zn abundances of all terrestrial basalts and Zn isotope compositions ($\delta^{66}Zn = +0.21 \pm 0.06$ ‰), generally lighter than for MORB ($\delta^{66}Zn = +0.28 \pm 0.06$ ‰). Accounting for partial melting, komatiites, boninites and MORB derive from mantle sources with $\delta^{66}Zn$ of ~0.16 ± 0.06 ‰. Lower-degree partial melts, such as alkali basalts, can have higher $\delta^{66}Zn$, with up to ~0.4 ‰ variation possible from partial melting of distinct peridotite mantle sources. Partial melting of fertile lherzolitic and depleted harzburgitic mantle sources can generate significant Zn isotope variability and should be evaluated prior to ascribing crustal, enriched or lithological components to mantle reservoirs from Zn compositions of planetary basalts.

Received 23 May 2022 | Accepted 23 August 2022 | Published 20 September 2022

Introduction

Zinc stable isotopes have utility in the study of basaltic rocks, from the examination of contributions of potential mantle and crustal reservoirs with distinct $^{66}Zn/^{64}Zn$ ratios (*e.g.*, Beunon *et al.*, 2020), to identification of volatile element loss in planets (*e.g.*, Paniello *et al.*, 2012). Zinc consists of five stable isotopes (^{64}Zn [natural abundance 48.6], ^{66}Zn [27.9], ^{67}Zn [4.1], ^{68}Zn [18.1], and ^{70}Zn [0.6]) which are typically reported in per mil variations relative to a standard ($\delta^{x}Zn = [(({}^{x}Zn/{}^{64}Zn)_{sample}/({}^{x}Zn/{}^{64}Zn)_{JMC\text{-}Lyon\ standard} - 1) \times 1000]$, where x typically refers to mass 66 or 68). Studies of basaltic magmatic differentiation series have demonstrated that Zn isotopes are not substantially modified (<0.1 ‰) during fractional crystallisation processes (Chen *et al.*, 2013), but that significant fractionation (≥0.1 ‰) in $\delta^{66}Zn$ is likely to occur during mantle partial melting (Wang *et al.*, 2017). Partial melting processes can explain $\delta^{66}Zn$ variations in arc lavas (Huang *et al.*, 2018), whereas it has been argued that $\delta^{66}Zn$ variations in some mantle-derived basaltic rocks reflect contributions from distinct sources, including recycled carbonate (Beunon *et al.*, 2020; Liu *et al.*, 2022).

Intraplate volcanic rocks, including ocean island basalts (OIB), were first used to estimate a bulk silicate Earth (BSE) Zn isotopic composition ($\delta^{66}Zn_{BSE} = +0.28 \pm 0.05$ ‰; all uncertainties 2 s.d.; Chen *et al.*, 2013), followed by direct analysis of fertile peridotites (+0.30 ± 0.03 ‰; Doucet *et al.*, 2016). Subsequently, peridotites and komatiites have been shown to have indistinguishable Zn isotopic compositions (+0.16 ± 0.06 ‰) and so were interpreted to represent a consistent $\delta^{66}Zn_{BSE}$ (Sossi *et al.*, 2018), with slightly more elevated estimates also reported from modern and ancient mantle melts (+0.20 ± 0.03 ‰; McCoy-West *et al.*, 2018; Doucet *et al.*, 2020), with a similar value established for depleted mid-ocean ridge basalt (MORB) mantle ($\delta^{66}Zn_{DMM} = +0.20 \pm 0.05$ ‰; Wang *et al.*, 2017). Observations of Zn isotope fractionation during partial melting (Wang *et al.*, 2017; Huang *et al.*, 2018) leave several outstanding questions prior to utilisation of Zn isotopes as tracers of distinct mantle and crustal reservoir contributions, and for estimating the BSE composition, particularly how Zn isotope variations differ in different melting regimes, such as during adiabatic decompression and during water-assisted mantle partial melting.

Limited data are available for Zn isotopes in MORB samples and data have yet to be reported for boninites. Boninites are potentially useful samples for understanding the behaviour of Zn during partial melting within the mantle. Unlike MORB, which are formed during adiabatic decompression melting, and hotspot volcanic rocks (OIB, komatiites) that are likely produced through thermal anomalies in the mantle, boninites are widely accepted to form from low pressure melting of previously depleted mantle sources by flux melting of water (*e.g.*, Cameron *et al.*, 1979; Crawford *et al.*, 1989). These rocks should therefore have low Zn and relatively isotopically light $\delta^{66}Zn$ due to their origin from refractory mantle similar to harzburgite (~+0.16 ‰; Doucet *et al.*, 2016; Wang *et al.*, 2017). An alternative possibility exists that boninites might show Zn isotope variations due to variable additions of pelagic sedimentary components or altered igneous rocks that are known to have affected

1. Scripps Institution of Oceanography, San Diego, La Jolla, CA 92093-0244, USA
2. Université Paris Cité, Institut de Physique du Globe de Paris, CNRS, 1 rue Jussieu, 75238 Paris, France
3. Institute of Earthquake and Volcano Geology, Geological Survey of Japan, AIST, Central 7, 1-1-1, Higashi, Tsukuba, Ibaraki 305-8567, Japan
* Corresponding author (email: jmdday@ucsd.edu)

them from Sr-Nd-Hf-Pb isotope studies (*e.g.*, Ishizuka *et al.*, 2020). The first boninite data are presented from Nakoudojima Island and the Bonin Ridge (Ishizuka *et al.*, 2011, 2014), Japan, along with a new dataset for MORB from three ocean basins (Atlantic, Indian, Pacific) that greatly expands existing MORB Zn isotope data, to further examine Zn behaviour during partial melting processes.

Methods and Results

Methods for the separation and analysis of Zn abundances and isotopic composition are described in detail in the Supplementary Information. Five boninite samples from the Izu-Bonin Mariana Arc, Japan, were analysed for Zn isotope and elemental abundances (Table 1) for which bulk rock major- and trace-element data has been published previously (Ishizuka *et al.*, 2011, 2014). These samples were erupted during the Eocene (44–48 Ma), span a range of MgO (4.4 to 15.2 wt. %) and SiO_2 contents (55.2 to 62.4 wt. %), and have trace element and isotopic compositions consistent with partial melts originating from depleted mantle sources. Boninites have between 20 and 52 ppm Zn and δ^{66}Zn from $+0.17 \pm 0.06$ to $+0.25 \pm 0.06$ ‰. Zinc isotope compositions are mass dependent and replicate analyses of KH07-2 D43 (Bonin Ridge) and 10100205 (Nakoudojima Island) provided identical results within uncertainties. Boninites have lower Zn abundances than MORB, OIB and most komatiites, and their average δ^{66}Zn ($+0.21 \pm 0.06$ ‰, 2 s.d.) is relatively homogeneous, similar to those measured for komatiites (Fig. S-1). For a given MgO content, boninites have the lowest Zn abundances and lie at the lowest values for δ^{66}Zn of all basaltic rocks (Fig. 1).

Zinc isotope data are reported for 22 mid-ocean ridge basalts spanning the Atlantic, Indian and Pacific Ocean basins in Table 1. Zinc isotope compositions fall along a mass-dependent slope and span a range in Zn abundances (40 to 93 ppm) yet a restricted range of δ^{66}Zn ($+0.28 \pm 0.06$ ‰; 2 s.d.), with no evidence for systematic variation between ocean basins. These results agree well with the limited range in δ^{66}Zn reported for MORB from the Atlantic and Indian oceans (Fig. S-1; Wang *et al.*, 2017), although the Zn abundances span a wider range.

Discussion

Boninite magmatism and the cause of low Zn and δ^{66}Zn. Partial melting occurs within shallow forearc regions during release of volatiles from the subducting slab into the mantle wedge and drives boninite magmatism (*e.g.*, Ishizuka *et al.*, 2011, 2014; Shervais *et al.*, 2021). Such melting produces high MgO (>8 wt. %), SiO_2 (52–63 wt. %), and low TiO_2 (<0.5 wt. %) melts distinct from komatiites, MORB, OIB or any other type of basaltic rock (*e.g.*, Crawford *et al.*, 1989), and which can be reproduced in melting experiments mimicking hydrous melting conditions of refractory harzburgite-like lithologies (Van der Laan *et al.*, 1989; Falloon and Danyushevsky, 2000). Forearc mantle is dominated by highly melt-depleted (residues after >20 % partial melting) harzburgite mantle formed by both modern and ancient melt events and is characterised by low Zn contents (Day and Brown, 2021), which can only be further melted by additions of fluids or excess temperatures. The fluid-assisted melting of such shallow depleted residues within the melting region of the nascent Izu-Bonin-Mariana subduction system in the Eocene is widely accepted as the cause of boninite magmatism at that time (Ishizuka *et al.*, 2011; Shervais *et al.*, 2021).

Doucet *et al.* (2016) and Wang *et al.* (2017) presented data for refractory harzburgites from a variety of continental lithospheric mantle localities for δ^{66}Zn, showing that they have generally similar Zn abundances to forearc harzburgites (~40 ppm) and lower δ^{66}Zn (~0.16 ‰) than lherzolites (~0.28 ‰; Fig. 1). Furthermore, analyses of minerals from spinel lherzolites indicate that olivine and orthopyroxene have lower δ^{66}Zn than clinopyroxene, or the main carrier of Zn, spinel, which is characterised by heavy δ^{66}Zn (Wang *et al.*, 2017). From these constraints, it is likely that boninite Zn systematics are a direct consequence of flux melting of low-Zn depleted harzburgites at low pressure.

Two potential issues are whether Zn can be affected by subducted pelagic sedimentary components or altered igneous rocks, and the possibility of mineral accumulation processes modifying Zn isotope systematics of boninites. Nakoudojima boninites have $^{87}Sr/^{86}Sr_i$ (0.7041–0.7049), $^{143}Nd/^{144}Nd_i$ (0.5127–0.5129) and Pb isotope systematics consistent with variable contamination from pelagic sediment (Ishizuka *et al.*, 2020). Drill core samples from the Bonin Ridge (*e.g.*, KH07-2 D43) have more MORB-like $^{87}Sr/^{86}Sr_i$ of 0.7031–0.7037 and $^{143}Nd/^{144}Nd_i$ of 0.5131–0.5132 (Ishizuka *et al.*, 2011). Despite the limited number of boninite samples studied, the large isotopic variations in Sr-Nd-Pb, yet limited range in Zn isotope ratios, suggest Zn in boninites is likely to be relatively unaffected by subducting sediment or altered igneous rock components. An alternative source for low δ^{66}Zn is accumulation of olivine with isotopically light Zn (McCoy-West *et al.*, 2018; Sossi *et al.*, 2018). This is not the case for boninites examined here, which do not contain significant accumulative olivine. Compared with komatiites, OIB, alkali basalts, basanites, and nephelinites, boninites plot at the lowest Zn and δ^{66}Zn for a given MgO of any terrestrial basaltic partial melt (Fig. 1). New data for MORB extend the range of Zn to abundances that can be as low as in boninites. This may indicate the presence of harzburgite source components in some MORB.

Mantle partial melting controls on Zn isotope fractionation. Due to their genesis in an unusual tectonic setting, boninites represent some of the largest-degree partial melts of all modern mantle-derived melts (Supplementary Information, Table 2). There are relationships between δ^{66}Zn and Zn and the extent of partial melting in basaltic rocks (Fig. 2). With decreasing extents of partial melting, both δ^{66}Zn and Zn concentrations tend to increase. An increase in incompatible ($D < 1$) Zn is expected at lower extents of partial melting, but the cause(s) of δ^{66}Zn increases are less clear. For example, this relationship could indicate obfuscation of components enriched in Zn with high δ^{66}Zn, such as recycled carbonates, at higher degrees of partial melting (Beunon *et al.*, 2020). Alternatively, such variations may result from melting variably depleted or fertile mantle peridotite without the obvious presence of recycled components, noting the difficulty in melting refractory mantle sources at low degrees of partial melting. To examine these possibilities, a family of non-modal partial melting models were constructed for Zn using previous modelling compilations (see Table S-1). The first assumes a fertile mantle garnet lherzolite composition (green lines) similar to that considered previously (*e.g.*, Sossi *et al.*, 2018); the second is a refractory mantle spinel harzburgite (red lines), and the third is a metasomatised mantle composition (blue lines) (Fig. 2).

Of interest for boninite petrogenesis is the refractory mantle harzburgite model. Assuming a starting composition similar to harzburgites presented by Doucet *et al.* (2016) this model yields Zn and δ^{66}Zn values within uncertainty of measured boninite compositions and expected degrees of partial melting (Fig. 2). The model supports the low Zn and δ^{66}Zn of boninites reflecting partial melting of refractory forearc mantle peridotites. MORB lie slightly above the partial melting estimates for spinel

Table 1 Zinc isotope and abundance data for boninites and mid-ocean ridge basalts. Major element data and ages for boninites are from Ishizuka *et al.* (2011, 2014) and for MORB are from Le Roux (2000) and Deng *et al.* (2018).

Sample	Location	Rock Type	Age (Ma)	Uncer.	SiO_2 (wt. %)	MgO (wt. %)	Zn (ppm)	$\delta^{66}Zn$ (‰)	±2σ	$\delta^{68}Zn$ (‰)	±2σ	*n*
10100202	Nakoudojima Island	Boninite	47.81	0.17	55.6	13.4	45.3	0.22	0.02	0.40	0.03	3
10100215	Nakoudojima Island	Boninite			55.2	15.2	50.7	0.17	0.06	0.34	0.09	4
10100213	Nakoudojima Island	Bronzite Andesite			57.1	7.1	19.9	0.25	0.06	0.45	0.10	4
10100205*	Nakoudojima Island	Basaltic Dike			58.2	6.7	49.8	0.20	0.07	0.40	0.05	4
							49.3	0.18	0.04	0.37	0.04	4
KH07-2 D43*	Bonin Ridge	Submarine boninite	44.78	0.16	62.4	4.4	51.8	0.21	0.05	0.43	0.10	4
							46.0	0.24	0.05	0.46	0.07	4
SWIFT DR32-1-3g	South West Indian Ridge	MORB					66.2	0.29	0.03	0.61	0.06	6
SWIFT DR04-2-3g	South West Indian Ridge	MORB				6.2		0.26	0.06	0.51	0.13	4
SWIFT DR06-3-6g	South West Indian Ridge	MORB				6.6	78.6	0.30	0.06	0.61	0.08	5
MD57 D2-8	Central Indian Ridge	MORB				5.8	60.4	0.31	0.03	0.62	0.09	6
MD57 D7-5	Central Indian Ridge	MORB				8.1	50.2	0.29	0.04	0.56	0.07	6
MD57 D9-4	Central Indian Ridge	MORB					59.8	0.26	0.05	0.52	0.11	5
EW9309 10D-3g	Mid Atlantic Ridge, 40–50°S	MORB			50.7	7.9	56.5	0.31	0.03	0.58	0.04	6
EW9309 27D-1g	Mid Atlantic Ridge, 40–50°S	MORB			49.0	8.3	40.3	0.26	0.06	0.56	0.11	5
EW9309 3D	S Atlantic (Discovery)	MORB			50.6	7.0		0.31	0.02	0.61	0.07	3
EW9309 20D*	S Atlantic (Discovery)	MORB			50.8	6.9		0.29	0.09	0.59	0.23	3
								0.24	0.03	0.47	0.03	2
RD87 DR18-102	North Atlantic (Dosso)	MORB				7.4	54.7	0.26	0.05	0.49	0.10	6
RD87 DR24	North Atlantic (Dosso)	MORB					56.4	0.27	0.06	0.50	0.11	6
RD87 DR29-107	North Atlantic (Dosso)	MORB					44.8	0.27	0.01	0.54	0.04	4
DIVA1 12-2	Mid Atlantic Ridge, 37–38°N	MORB					49.6	0.35	0.03	0.72	0.04	6
DIVA1 13-3	Mid Atlantic Ridge, 37–38°N	MORB				7.6	60.2	0.33	0.04	0.62	0.07	6
DIVA1 15-5	Mid Atlantic Ridge, 37–38°N	MORB				5.9	75.9	0.27	0.06	0.52	0.11	5
PAC2 DR32-1g	Pacific-Antarctic Ridge	MORB				6.2	90.6	0.24	0.01	0.49	0.03	2
PAC2 DR37-3g	Pacific-Antarctic Ridge	MORB					75.3	0.24	0.06	0.48	0.09	4
PAC2 DR38-1g	Pacific-Antarctic Ridge	MORB				7.6	70.1	0.27	0.02	0.55	0.06	4
SEARISE1 DR04	East Pacific Rise	MORB			50.0	6.8	92.8	0.25	0.03	0.48	0.04	5
SEARISE2 DR03	East Pacific Rise	MORB			51.2	7.3	62.0	0.28	0.06	0.54	0.09	6
CYP 12-34	East Pacific Rise	MORB			50.4	8.2	65.8	0.27	0.05	0.51	0.08	5

*Replicate analyses are reported for these samples.

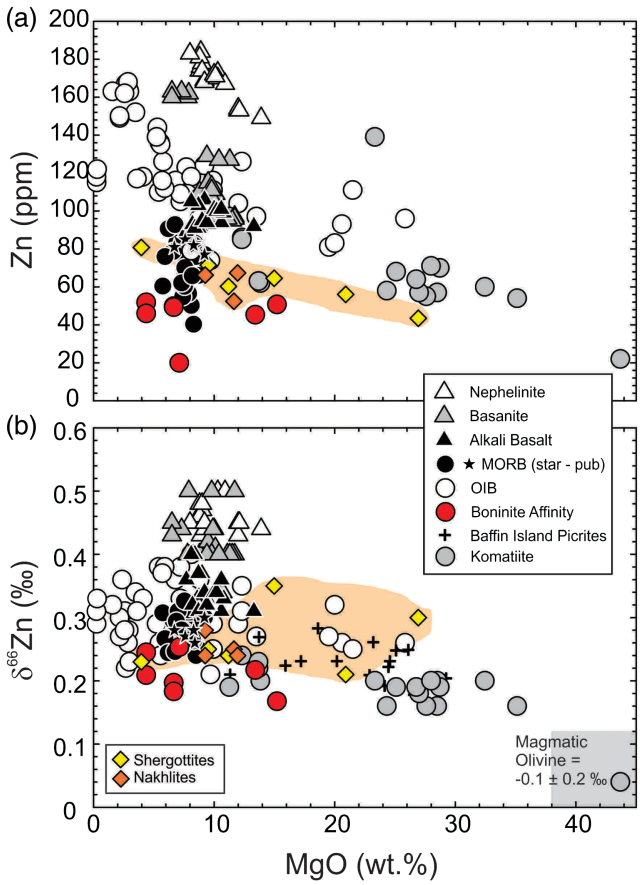

Figure 1 Bulk rock **(a)** Zn abundance and **(b)** isotopic composition as a function of MgO content for basaltic rocks. Data sources are given in Figure S-1, with Baffin Island bulk rock picrite data and the magmatic olivine compositions (assuming a possible range of olivine MgO contents) from McCoy-West *et al.* (2018). Martian shergottite and nakhlite data (shown as points and as a field) are from Paniello *et al.* (2012). New MORB data presented here (solid circles) are distinguished from published data (solid stars).

harzburgite, yet are also consistent with generation from a relatively refractory mantle source, as would be expected for melts of DMM. Conversely, the fertile lherzolite mantle composition of Doucet *et al.* (2016) can reproduce the Zn abundances observed in OIB and komatiites, but not the δ^{66}Zn of komatiites, where a low δ^{66}Zn source, more akin to refractory harzburgite, better matches komatiite data. OIB span a range of compositions that could be explained by mixtures of both refractory and fertile peridotite sources. Conversely, low-degree partial melts like alkali basalts, basanites and nephelinites from eastern China (Wang *et al.*, 2018) require fertile melt compositions, but their high Zn abundances also permit contributions from hybridised metasomatised peridotite mantle sources.

Mantle-derived basaltic rocks can span ~0.4 ‰ variation in δ^{66}Zn. In the absence of other evidence, such as O-Ca-Sr-Nd-Os-Pb isotopic variability reflecting distinct mantle or crustal components, much of the variation in Zn isotopes can be attributed to different extents of partial melting of variably fertile and refractory peridotite mantle sources. Studies using Zn isotopes to examine potential carbonate or enriched recycled mantle sources in OIB and related rocks should consider the potential for partial melting control on Zn isotope fractionation. Relatively low degree partial melts are likely to sample more extreme end member compositions for Zn. The highest degree partial melts

Table 2 Zinc isotope, abundance data, melting type and extent for terrestrial basalts.

Rock Type	Melting Process	Partial Melting Extent	Estimate (%)	Location	δ^{66}Zn (‰)	±2σ	Av. Zn (ppm)	Range Zn (ppm)	*n*	Data Sources
Komatiite	High- to low-*P* high-*T* Melting	<30–50 %	40 ± 10	Plume?	0.16	0.06	66	22–139	18	Sossi *et al.* (2018); Herzberg (1992)
Boninite	Low-*P* Flux Melting	12–23 %	18 ± 8	Forearc	0.21	0.06	45	20–52	5	This study; Shervais *et al.* (2021)
MORB	Adiabatic Decompression	~10 %	10 ± 4	Ridge	0.28	0.06	64	40–93	28	This study; Wang *et al.* (2017)
OIB	High-*T* Melting	2–10 %	5 ± 4	Plume	0.30	0.10	120	81–165	57	Chen *et al.* (2013); Wang *et al.* (2017)
Alkali Basalt	Low-degree melt	<4 %	4 ± 2	Various	0.34	0.06	96	91–106	18	Wang *et al.* (2018)
Basanite	Low-degree melt	<3 %	3 ± 2	Various	0.42	0.08	122	95–163	20	Wang *et al.* (2018)
Nephelinite	Low-degree melt	<2 %	2 ± 1	Various	0.45	0.06	168	149–184	19	Wang *et al.* (2018)

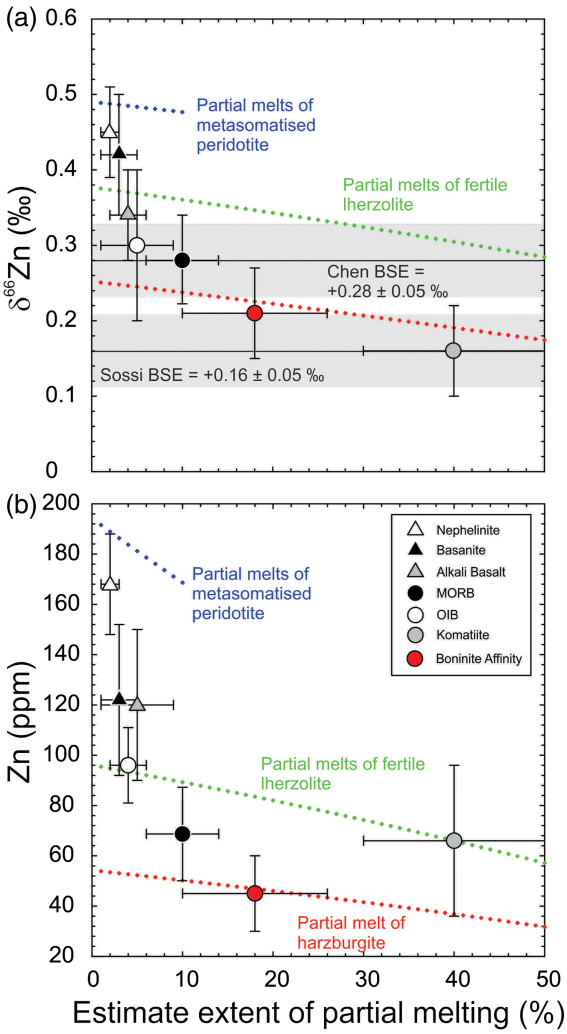

Figure 2 **(a)** Zinc isotopic composition and **(b)** Zn abundance *versus* estimated degree of partial melting for basaltic rocks (Table 2) *versus* models for partial melting of harzburgite, lherzolite and metasomatised peridotite, with dots conforming to 1 % increments of melting. Shown in upper panel are the estimated bulk silicate Earth (BSE) average (solid line) and standard deviation (shaded regions) values from Chen *et al.* (2013) and Sossi *et al.* (2018).

examined are MORB, boninites and komatiites, and these necessarily sample the largest regions of mantle and so are most likely to express mantle composition. Based on data trends and models, these magmatic rocks appear to sample mantle sources akin to harzburgite mantle for δ^{66}Zn. In this sense, high degree partial melts from ancient (komatiites) and modern (boninites, MORB) magmatism conform to the value determined by Sossi *et al.* (2018) of +0.16 ± 0.06 ‰, consistent with BSE being perhaps up to +0.2 ‰ (*e.g.*, McCoy-West *et al.*, 2018; Doucet *et al.*, 2020).

It has been shown that basaltic rocks from the Moon have δ^{66}Zn values ~1 ‰ heavier and Zn abundances >20 times less than terrestrial basalts, interpreted to reflect volatile loss during lunar formation (Paniello *et al.*, 2012). Such large differences between basalts from the Earth and Moon cannot be reconciled by differences in extents of partial melting. Paniello *et al.* (2012) also presented Zn isotope data for martian meteorites (Fig. 1). Shergottites are relatively high-degree basaltic partial melts of depleted and enriched mantle sources in Mars, while nakhlites have been considered akin to rejuvenated lava, which are formed by lower degrees of partial melting, meaning the closest analogues to these samples are plume-derived melts on Earth (Day *et al.*, 2018). Martian meteorites have low Zn contents and δ^{66}Zn in the upper range of terrestrial plume-derived lavas (OIB, komatiites) for a given MgO content. Such results are consistent with lower Zn contents in bulk silicate Mars and may suggest a slightly heavier bulk silicate Mars value for δ^{66}Zn compared to Earth. This conclusion needs to be confirmed by further analyses of martian meteorites.

Acknowledgements

Reviews by L. Doucet and an anonymous referee are appreciated. An Institut de Physique du Globe de Paris Visiting Professor position (JMDD), ERC grant agreement No. 101001282 (METAL), the UnivEarthS Labex program (numbers: ANR-10-LABX-0023 and ANR-11-IDEX-0005-02), the IPGP multidisciplinary program PARI, and the Region île-de-France DIM ACAV + and SESAME Grants no. 12015908 supported this work.

Editor: Anat Shahar

Additional Information

Supplementary Information accompanies this letter at https://www.geochemicalperspectivesletters.org/article2230.

Cite this letter as: Day, J.M.D, Moynier, F., Ishizuka, O. (2022) A partial melting control on the Zn isotope composition of basalts. *Geochem. Persp. Let.* 23, 11–16. https://doi.org/10.7185/geochemlet.2230

References

Beunon, H., Mattielli, N., Doucet, L.S., Moine, B., Debret, B. (2020) Mantle heterogeneity through Zn systematics in oceanic basalts: Evidence for a deep carbon cycling. *Earth-Science Reviews* 205, 103174. https://doi.org/10.1016/j.earscirev.2020.103174

Cameron, W.E., Nisbet, E.G., Dietrich, V.J. (1979) Boninites, komatiites and ophiolitic basalts. *Nature* 280, 550–553. https://doi.org/10.1038/280550a0

Chen, H., Savage, P.S., Teng, F.-Z., Helz, R.T., Moynier, F. (2013) Zinc isotope fractionation during magmatic differentiation and the isotopic composition of the bulk Earth. *Earth and Planetary Science Letters* 369–370, 32–42. https://doi.org/10.1016/j.epsl.2013.02.037

Crawford, A.J., Falloon, T.J., Green, D.H. (1989) Classification, petrogenesis and tectonic setting of boninites. In: Crawford, A.J. (Ed.) *Boninites and Related Rocks*. Unwin Hyman, London, 1–49.

Day, J.M.D., Brown, D.B. (2021) Ancient Melt-Depletion in Fresh to Strongly Serpentinized Tonga Trench Peridotites. *Journal of Petrology* 62, egab088. https://doi.org/10.1093/petrology/egab088

Day, J.M.D., Tait, K.T., Udry, A., Moynier, F., Liu, Y., Neal, C.R. (2018) Martian magmatism from plume metasomatized mantle. *Nature Communications* 9, 4799. https://doi.org/10.1038/s41467-018-07191-0

Deng, Z., Moynier, F., Sossi, P.A., Chaussidon, M. (2018) Bridging the depleted MORB mantle and the continental crust using titanium isotopes.

Geochemical Perspectives Letters 9, 11–15. https://doi.org/10.7185/geochemlet.1831

Doucet, L.S., Mattielli, N., Ionov, D.A., Debouge, W., Golovin, A.V. (2016) Zn isotopic heterogeneity in the mantle: A melting control? *Earth and Planetary Science Letters* 451, 232–240. https://doi.org/10.1016/j.epsl.2016.06.040

Doucet, L.S., Laurent, O., Ionov, D.A., Mattielli, N., Debaille, V., Debouge, W. (2020) Archean lithospheric differentiation: Insights from Fe and Zn isotopes. *Geology* 48, 1028–1032. https://doi.org/10.1130/G47647.1

Falloon, T.J., Danyushevsky, L.V. (2000) Melting of Refractory Mantle at 1.5, 2 and 2.5 GPa under Anhydrous and H_2O-undersaturated Conditions: Implications for the Petrogenesis of High-Ca Boninites and the Influence of Subduction Components on Mantle Melting. *Journal of Petrology* 41, 257–283. https://doi.org/10.1093/petrology/41.2.257

Herzberg, C. (1992) Depth and degree of melting of komatiites. *Journal of Geophysical Research: Solid Earth* 97, 4521–4540. https://doi.org/10.1029/91JB03066

Huang, J., Zhang, X.-C., Chen, S., Tang, L., Wörner, G., Yu, H., Huang, F. (2018) Zinc isotopic systematics of Kamchatka-Aleutian arc magmas controlled by mantle melting. *Geochimica et Cosmochimica Acta* 238, 85–101. https://doi.org/10.1016/j.gca.2018.07.012

Ishizuka, O., Tani, K., Reagan, M.K., Kanayama, K., Umino, S., Harigane, Y., Sakamoto, I., Miyajima, Y., Yuasa, M., Dunkley, D.J. (2011) The timescales of subduction initiation and subsequent evolution of an oceanic island arc. *Earth and Planetary Science Letters* 306, 229–240. https://doi.org/10.1016/j.epsl.2011.04.006

Ishizuka, O., Umino, S., Taylor, R.N., Kanayama, K. (2014) Evidence for Hydrothermal Activity in the Earliest Stages of Intraoceanic Arc Formation: Implications for Ophiolite-Hosted Hydrothermal Activity. *Economic Geology* 109, 2159–2178. https://doi.org/10.2113/econgeo.109.8.2159

Ishizuka, O., Taylor, R.N., Umino, S., Kanayama, K. (2020) Geochemical Evolution of Arc and Slab Following Subduction Initiation: a Record from the Bonin Islands, Japan. *Journal of Petrology* 61, egaa050. https://doi.org/10.1093/petrology/egaa050

Le Roux, P.J. (2000) The geochemistry of selected mid-ocean ridge basalts from the Southern mid-Atlantic ridge (40°-55°S). PhD Thesis, University of Cape Town. https://open.uct.ac.za/handle/11427/4207

Liu, S.A., Qu, Y.R., Wang, Z.Z., Li, M.L., Yang, C., Li, S.G. (2022) The fate of subducting carbon tracked by Mg and Zn isotopes: A review and new perspectives. *Earth-Science Reviews* 228, 104010. https://doi.org/10.1016/j.earscirev.2022.104010

McCoy-West, A.J., Fitton, J.G., Pons, M.L., Inglis, E.C., Williams, H.M. (2018) The Fe and Zn isotope composition of deep mantle source regions: Insights from Baffin Island picrites. *Geochimica et Cosmochimica Acta* 238, 542–562. https://doi.org/10.1016/j.gca.2018.07.021

Paniello, R.C., Day, J.M.D., Moynier, F. (2012) Zinc isotopic evidence for the origin of the Moon. *Nature* 490, 376–379. https://doi.org/10.1038/nature11507

Shervais, J.W., Reagan, M.K., Godard, M., Prytulak, J., Ryan, J.G., *et al.* (2021) Magmatic Response to Subduction Initiation, Part II: Boninites and Related Rocks of the Izu-Bonin Arc From IODP Expedition 352. *Geochemistry, Geophysics, Geosystems* 22, e2020GC009093. https://doi.org/10.1029/2020GC009093

Sossi, P.A., Nebel, O., O'Neill, H.S.C., Moynier, F. (2018) Zinc isotope composition of the Earth and its behaviour during planetary accretion. *Chemical Geology* 477, 73–84. https://doi.org/10.1016/j.chemgeo.2017.12.006

Van der Laan, S.R., Flower, M.J.F., Koster van Groos, A.F. (1989) Experimental evidence for the origin of boninites: near-liquidus phase relations to 7.5 kbar. In: Crawford, A.J. (Ed.) *Boninites and Related Rocks*. Unwin Hyman, London, 112–147.

Wang, Z.-Z., Liu, S.-A., Liu, J., Huang, J., Xiao, Y., Chu, Z.-Y., Zhao, X.-M., Tang, L. (2017) Zinc isotope fractionation during mantle melting and constraints on the Zn isotope composition of Earth's upper mantle. *Geochimica et Cosmochimica Acta* 198, 151–167. https://doi.org/10.1016/j.gca.2016.11.014

Wang, Z.-Z., Liu, S.-A., Chen, L.-H., Li, S.-G., Zeng, G. (2018) Compositional transition in natural alkaline lavas through silica-undersaturated melt–lithosphere interaction. *Geology* 46, 771–774. https://doi.org/10.1130/G45145.1

Geochemical Perspectives Letters

A partial melting control on the Zn isotope composition of basalts

J.M.D. Day, F. Moynier, O. Ishizuka

Supplementary Information

The Supplementary Information includes:

- Methods
- Partial Melting Estimates
- Partial Melting Model
- Table S1
- Figure S1
- Supplementary References

Methods

One hundred and fifty milligram aliquots of powdered boninite and ~30–60 mg of MORB glass were digested in mixtures of ultra-pure 4 parts HF and 1 part HNO_3 in Teflon beakers for 48 hours on a hotplate at 140 °C. Samples were dried down and 6 mol/L ultra-pure HCl was added to dissolve aliquots for another 24 hours at 140 °C on the hotplate. Purification of Zn was achieved using an improved anion-exchange chromatography method, with a recovery of 99.99 % (van Kooten and Moynier, 2019). Samples were loaded in 1.5 mol/L HBr on 0.1 mL AG1-X8 (200–400 mesh) ion-exchange columns with Zn being collected in 0.5 mol/L HNO_3. This step was repeated to purify Zn fractions. A procedural blank measured with samples was 0.2 ng, representing less than 0.1 % of total measured Zn for samples. Isotopic compositions of Zn were measured on the *Thermo Fisher* Neptune Plus multi-collector inductively coupled plasma mass spectrometer (MC-ICP-MS) housed at the Institut de Physique du Globe de Paris. Faraday cups were positioned to collect ions on masses 62, 63, 64, 65, 66, 67 and 68. Possible ^{64}Ni isobaric interferences were corrected by measuring the intensity of the ^{62}Ni peak. A solution containing 10 ppb Zn in 0.1 mol/L HNO_3 was prepared for isotopic analysis. Isotopic ratios of Zn in samples were analysed using an Apex IR introduction system, combined with a 100 L/min PFA nebuliser following van Kooten and Moynier (2019). A single block of 30 ratios, in which the integration time of one scan was 8.3 seconds, was measured for each sample. Background was corrected by subtracting the on-

peak zero intensities from a blank solution. The instrumental mass bias was corrected by bracketing each of the samples with standards. BHVO-2 and AGV-2 gave $\delta^{66}Zn$ = +0.30 ± 0.04 ‰ ($\delta^{68}Zn$ = +0.64 ± 0.06 ‰; 100.2 ppm Zn; n = 4) and $\delta^{66}Zn$ = +0.25 ± 0.08 ‰ ($\delta^{68}Zn$ = +0.53 ± 0.08 ‰; n = 6) respectively, consistent with recommended values (Moynier *et al*., 2017).

Partial Melting Estimates

Based on rare earth element modelling, Shervais *et al*. (2021) demonstrated that boninites form from between ~12 and 23 % partial melting of already refractory harzburgite, dominantly from shallow (spinel stability field) melting. Such high degrees of partial melting are uncommon in the Phanerozoic but were more common in the Archaean where komatiites were generated by as much as 40 ± 10 % partial melting of likely more fertile mantle sources (*e.g.*, Herzberg, 1992). To examine the role of partial melting on Zn isotope fractionation, we compare these extreme endmember rock types with modern mantle-derived basalts from a range of tectonic settings which show a range of MgO contents, Zn abundances and $\delta^{66}Zn$ (Figures 1, S1). Partial melting estimates (Table 2) are conservative estimates of melting, including for MORB (*e.g.*, Asimow *et al.,* 2001), and alkali basalts to nephelinites, the latter of which can be produced by very low degree partial melting of CO_2-bearing lherzolite (*e.g.*, Foley *et al.,* 2009).

Partial Melting Model

Prior workers have developed partial melting models for partial melting of fertile spinel peridotites (Sossi *et al.*, 2018) as well as melting of garnet facies mantle (McCoy-West *et al.*, 2018) and we followed their overall protocol. We developed several partial melting models, using the experimentally determined mineral/melt partitioning for Zn from Davis *et al.* (2013) and utilising melt assemblage starting fractions and melting reactions for spinel peridotite from Wasylenki *et al.* (2003) and garnet peridotite from Walter (1998). We used olivine-orthopyroxene-clinopyroxene-garnet isotope fractionation factors taken from Sossi *et al.* (2018) and McCoy-West *et al.* (2018). Due to the requirement to model both depleted (*i.e.* harzburgitic) and fertile (*i.e.* lherzolitic) partial melting, we used separate model parameters given in Table S1. In addition, we modelled partial melts of metasomatised peridotite. Metasomatised peridotite could vary significantly in modal composition, and we elected to model a composition that only varied cryptically from fertile garnet peridotite, by modifying melting modes and initial starting composition of Zn. We acknowledge that other possibilities exist and could be equally—or more—suitable with our model given solely to exemplify what metasomatism might do for Zn abundances and isotopic compositions in some low degree partial melts.

Supplementary Table

Table S-1 Parameters used in modelling for Figure 2.

Phase	Partitioning	D_{Zn}[a]	$\Delta^{66}Zn$ (‰)[b]	Refractory Mantle		Fertile Mantle		Hybridised Mantle	
				Harz. Starting Fraction[c]	Harz. Melting Reaction[c]	Lherz. Starting Fraction[c]	Lherz. Melting Reaction[c]	MP Starting Fraction[c]	MP Melting Reaction[c]
Olivine	Ol-melt	0.96	$-0.17 \times 10^6/T^2$	0.6	−0.25	0.52	−0.25	0.52	−0.20
Opx	Opx-melt	0.451	$-0.17 \times 10^6/T^2$	0.38	0.35	0.22	0.35	0.22	0.20
Cpx	Cpx-melt	0.333	$-0.17 \times 10^6/T^2$	0	0.8	0.16	0.8	0.16	0.80
Garnet	Grt-melt	0.213	$-0.2 \times 10^6/T^2$	0	–	0.10	0.10	0.10	0.20
Spinel	Sp-melt	5.2	$0 \times 10^6/T^2$	0.02	0.10	0	–	0	–
Initial Zn (ppm) source[d]				40		65		102	
Initial $\delta^{66}Zn$ (‰) source[d]				0.16		0.28		0.42	

[a] Partition coefficients for Zn from Davis *et al.* (2013).

[b] Isotope fractionation factors after work of McCoy-West *et al.* (2018) and Sossi *et al.* (2018).

[c] Starting (modal abundance) fraction and melting reaction values are modified from Walter (1998) and Wasylneki *et al.* (2003).

[d] Initial Zn isotope and abundances for the lherzolite and harzburgite come from average of Doucet *et al.* (2016) data. The metasomatised peridotite (MP) mimicks CL9-078 of Wang *et al.* (2017).

Supplementary Figure

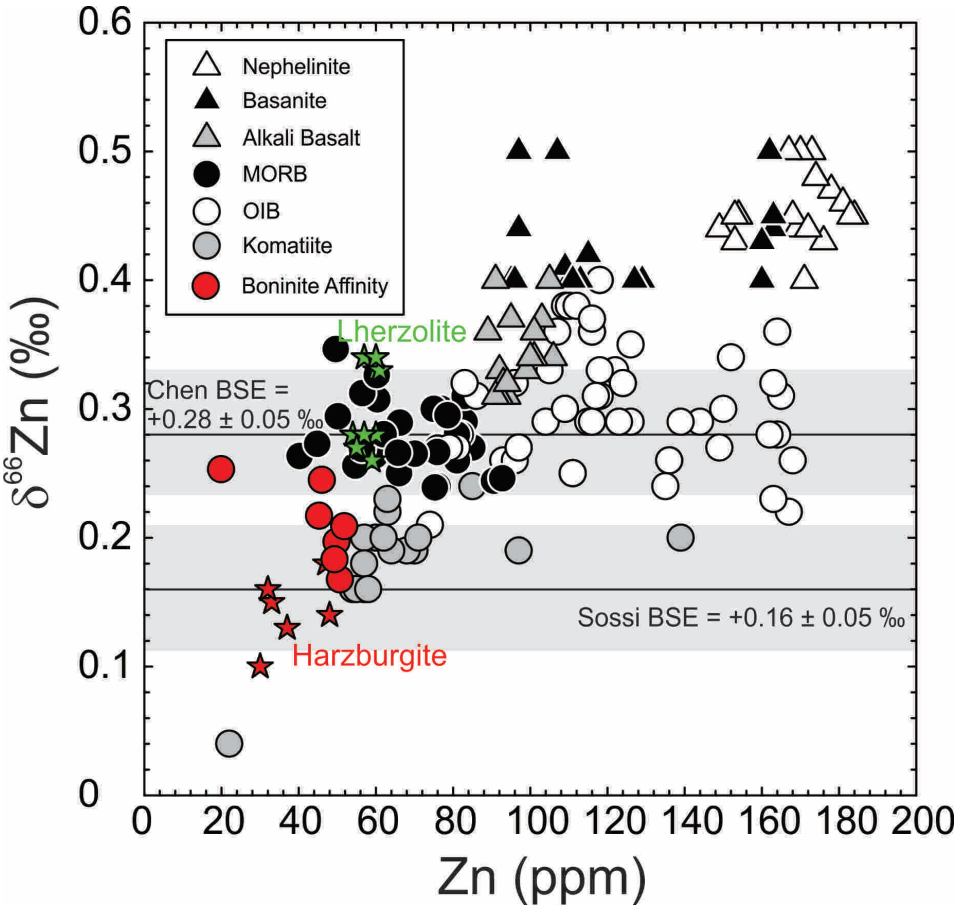

Figure S-1 Zinc isotopic composition as a function Zn abundance for bulk rock samples boninites *versus* low-degree partial melts (nephelinite, basanite, alkali basalt) from Wang *et al.* (2018), mid-ocean ridge basalts (MORB; Wang *et al.*, 2017; this study), ocean island basalts (OIB; Chen *et al.*, 2013; Wang *et al.*, 2017), and komatiites (Sossi *et al.*, 2018) along with fertile lherzolite and depleted harzburgite xenoliths (Doucet *et al.*, 2016). Shown are the estimated bulk silicate Earth (BSE) average (solid line) and standard deviation (shaded regions) values from Chen *et al.* (2013) and Sossi *et al.* (2018).

Supplementary Information References

Asimow, P.D., Hirschmann, M.M., Stolper, E.M. (2001) Calculation of Peridotite Partial Melting from Thermodynamic Models of Minerals and Melts, IV. Adiabatic Decompression and the Composition and Mean Properties of Mid-ocean Ridge Basalts. *Journal of Petrology* 42, 963–998. https://doi.org/10.1093/petrology/42.5.963

Chen, H., Savage, P.S., Teng, F.-Z., Helz, R.T., Moynier, F. (2013) Zinc isotope fractionation during magmatic differentiation and the isotopic composition of the bulk Earth. *Earth and Planetary Science Letters* 369–370, 32–42. https://doi.org/10.1016/j.epsl.2013.02.037

Davis, F.A., Humayun, M., Hirschmann, M.M., Cooper, R.S. (2013) Experimentally determined mineral/melt partitioning of first-row transition elements (FRTE) during partial melting of peridotite at 3 GPa. *Geochimica et Cosmochimica Acta* 104, 232–260. https://doi.org/10.1016/j.gca.2012.11.009

Doucet, L.S., Mattielli, N., Ionov, D.A., Debouge, W., Golovin, A.V. (2016) Zn isotopic heterogeneity in the mantle: A melting control? *Earth and Planetary Science Letters* 451, 232–240. https://doi.org/10.1016/j.epsl.2016.06.040

Foley, S.F., Yaxley, G.M., Rosenthal, A., Buhre, S., Kiseeva, E.S., Rapp, R.P., Jacob, D.E. (2009) The composition of near-solidus melts of peridotite in the presence of CO_2 and H_2O between 40 and 60 kbar. *Lithos* 112, 274–283. https://doi.org/10.1016/j.lithos.2009.03.020

Herzberg, C. (1992) Depth and degree of melting of komatiites. *Journal of Geophysical Research: Solid Earth* 97, 4521–4540. https://doi.org/10.1029/91JB03066

McCoy-West, A.J., Fitton, J.G., Pons, M.L., Inglis, E.C., Williams, H.M. (2018) The Fe and Zn isotope composition of deep mantle source regions: Insights from Baffin Island picrites. *Geochimica et Cosmochimica Acta* 238, 542–562. https://doi.org/10.1016/j.gca.2018.07.021

Moynier, F., Vance, D., Fujii, T., Savage, P. (2017) The Isotope Geochemistry of Zinc and Copper. *Reviews in Mineralogy and Geochemistry* 82, 543–600. https://doi.org/10.2138/rmg.2017.82.13

Shervais, J.W., Reagan, M.K., Godard, M., Prytulak, J., Ryan, J.G., *et al.* (2021) Magmatic Response to Subduction Initiation, Part II: Boninites and Related Rocks of the Izu-Bonin Arc From IODP Expedition 352. *Geochemistry, Geophysics, Geosystems* 22, e2020GC009093. https://doi.org/10.1029/2020GC009093

Sossi, P.A., Nebel, O., O'Neill, H.S.C., Moynier, F. (2018) Zinc isotope composition of the Earth and its behaviour during planetary accretion. *Chemical Geology* 477, 73–84. https://doi.org/10.1016/j.chemgeo.2017.12.006

van Kooten, E., Moynier, F. (2019) Zinc isotope analyses of singularly small samples (<5 ng Zn): Investigating chondrule-matrix complementarity in Leoville. *Geochimica et Cosmochimica Acta* 261, 248–268. https://doi.org/10.1016/j.gca.2019.07.022

Walter, M.J. (1998) Melting of Garnet Peridotite and the Origin of Komatiite and Depleted Lithosphere. *Journal of Petrology* 39, 29–60. https://doi.org/10.1093/petroj/39.1.29

Wang, Z.-Z., Liu, S.-A., Liu, J., Huang, J., Xiao, Y., Chu, Z.-Y., Zhao, X.-M., Tang, L. (2017) Zinc isotope fractionation during mantle melting and constraints on the Zn isotope composition of Earth's upper mantle. *Geochimica et Cosmochimica Acta* 198, 151–167. https://doi.org/10.1016/j.gca.2016.11.014

Wang, Z.-Z., Liu, S.-A., Chen, L.-H., Li, S.-G., Zeng, G. (2018) Compositional transition in natural alkaline lavas through silica-undersaturated melt–lithosphere interaction. *Geology* 46, 771–774. https://doi.org/10.1130/G45145.1

Wasylenki, L.E., Baker, M.B., Kent, A.J.R., Stopler, E.M. (2003) Near-solidus Melting of the Shallow Upper Mantle: Partial Melting Experiments on Depleted Peridotite. *Journal of Petrology* 44, 1163–1191. https://doi.org/10.1093/petrology/44.7.1163